C. R. Chimie 17 (2014) 641–655

Contents lists available at ScienceDirect

Comptes Rendus Chimie

www.sciencedirect.com

Account/Revue

Nanocast mesoporous mixed metal oxides for catalytic applications☆

Nanomoulage d'oxydes mixtes mésoporeux pour des applications catalytiques

Mahesh Muraleedharan Nair, Hoang Yen, Freddy Kleitz *

Department of Chemistry and Centre de Recherche sur les Matériaux Avancés (CERMA), Université Laval, 1045, avenue de la Médecine, Quebec City, G1V 0A6 Canada

ARTICLE INFO

Article history:
Received 7 February 2014
Accepted after revision 17 April 2014
Available online 11 June 2014

Keywords:
Nanocasting
Mixed metal oxides
High surface area
Oxidation
Hydrogen
Perovskites

ABSTRACT

Since the initial discovery of ordered mesoporous silica in early 1990s, considerable innovations were achieved regarding their synthesis, characterization and applications. One of the best outcomes of these intense research efforts is the development of a solid templating method called "nanocasting", which is based on using mesoporous silica (or carbon) as a rigid template. This solid-to-solid replication method opened the pathway for synthesizing high surface area non-silica mesostructured materials that are challenging to obtain through conventional self-assembly processes which are based on amphiphilic *soft* structure-directing agents. In particular, the replicated metal oxide mesostructures obtained by this method were found to be highly versatile for a wide range of applications, especially in catalysis, owing to their large specific surface area. Furthermore, the nanocasting method is particularly suited for the synthesis of mixed metal compositions, favored by the possible confinement of mixed precursors in the nanopores of the template. In this account, we discuss some of the recent developments regarding the synthesis of nanocast mixed metal oxides and their perspectives of catalytic applications. It is here the choice of the authors to place emphasis on a few representative examples of compositions (e.g., non-noble metal-based catalysts, perovskites) and catalytic reactions (e.g., hydrogen production, gas-phase oxidation).

© 2014 Académie des sciences. Published by Elsevier Masson SAS. All rights reserved.

Mots clés :
Nanomoulage
Oxydes métalliques mixtes
Surface spécifique
Oxydation
Hydrogène
Pérovskites

RÉSUMÉ

Depuis la découverte de la silice mésoporeuse ordonnée au début des années 1990, des innovations considérables ont été réalisées en ce qui concerne leur synthèse, leur caractérisation et leurs applications. L'un des meilleurs résultats de ces intenses efforts de recherche est le développement d'une méthode de préparation appelée « nano-moulage », qui est basée sur l'utilisation de la silice mésoporeuse (ou de carbone) comme moule. Cette méthode, par réplication solide–solide, a ouvert la voie vers la synthèse de matériaux mésostructurés non siliciques de grande surface spécifique, qui sont difficiles à obtenir par

☆ Thematic issue dedicated to François Garin.

* Corresponding author.
E-mail address: freddy.kleitz@chm.ulaval.ca (F. Kleitz).

http://dx.doi.org/10.1016/j.crci.2014.04.005
1631-0748/© 2014 Académie des sciences. Published by Elsevier Masson SAS. All rights reserved.

le biais des processus d'autoassemblage moléculaire, basés quant à eux sur l'utilisation d'agents structurants comme les amphiphiles. En particulier, les oxydes métalliques mésostructurés obtenus par cette méthode de réplication peuvent être utilisés dans une large gamme d'applications, en particulier en catalyse, en raison de leur forte surface spécifique. De plus, la méthode de préparation par nano-moulage est particulièrement adaptée à la préparation des oxydes mixtes. La formation d'oxyde mixte est favorisée par le confinement des différents précurseurs des oxydes dans les nanopores de la matrice mésoporeuse. Dans cette revue, nous discuterons les récents développements concernant la préparation d'oxydes métalliques mixtes par la technique de « nano-moulage » et de leurs perspectives d'application en catalyse hétérogène. Le choix des auteurs est ici de mettre l'accent sur quelques exemples représentatifs (par exemple, les catalyseurs à base de métaux non précieux, les pérovskites) et un choix de réactions catalytiques comme la production d'hydrogène ou l'oxydation en phase gazeuse.

© 2014 Académie des sciences. Publié par Elsevier Masson SAS. Tous droits réservés.

1. Introduction

Significant progress has been made since the initial report of highly ordered mesoporous silica by the Mobil Company in 1992 [1], regarding the cooperative surfactant self-assembly templating method for the synthesis of mesoporous siliceous materials. However, the extension of this synthetic strategy towards the development of non-siliceous counterparts faced additional challenges [2]. Great progress was achieved later for the synthesis of various mesoporous carbon materials, exhibiting high degree of mesostructural order and controlled porosity, using similar soft-templating methods [3–5]. On the other hand, in the case of metal oxide compositions, the difficulty in controlling the hydrolysis and polymerization of the metal precursors still often led to the formation of materials with very poor structural order and low thermal stability after removal of the organic surfactant template [2]. Therefore, as an alternative to surfactants, the template may also be a solid with structural pores in which another solid is created, serving thus as a solid scaffold. In this method, a porous solid material is used as a rigid matrix, *i.e.*, its pores are filled with one or more precursor species which will react inside the pores to form the desired material. The matrix is subsequently removed to yield the product as a sort of ''replica''. In analogy to macroscopic techniques, this process can be termed *nanocasting*, *i.e.*, casting on the nanometric length, the porous matrix being the ''*mold*'' and the replicated product being the ''(*nano*)-*cast*''. Using this strategy, disordered porous carbons had already been obtained in the middle of the 1980s by using silica particles as templates [6]. Since then, nanocasting approaches have permitted the synthesis of a large variety of ordered mesoporous materials, such as carbons, noble metals, metal oxides, polymers, carbides, chalcogenides, nitrides, etc. [7–15]. Ordered mesoporous silica materials are now serving widely as the templates for nanocasting procedures. Especially, solid templates such as SBA-15, KIT-6 and SBA-16 are the most frequently chosen because of their high porosity, large pore walls, and 3-D pore network interconnectivity [16–22]. This method is becoming increasingly popular and used commonly nowadays for the preparation of functional porous materials for applications in sensing, magnetic materials, materials for energy storage and conversion, catalysis, and so forth. Excellent reviews summarizing the advances on nanocasting are available elsewhere [16–22].

The use of ordered mesoporous materials as hard templates has several advantages when compared to direct soft-templating strategies. First, many ordered porous materials simply cannot be synthesized by soft-templating. For example, only a limited range of mesoporous metal oxides and metals have successfully been prepared by utilization of amphiphilic structure-directing agents [18,22]. Differently, the nanocasting approach is proven to be highly suitable for the preparation of mesostructured metal oxides of various compositions that are usually impossible or difficult to prepare by the direct templating methods because of their poor redox stability. As a few examples, ordered mesoporous oxides such as In_2O_3, Co_3O_4, Fe_2O_3, CeO_2, Cr_2O_3, NiO, WO_3, etc. are all accessible by replication of ordered mesoporous silica materials [9–14,23–29]. Moreover, the framework walls of these templated mesoporous oxides are composed of crystalline nanoparticles in most of the reported cases; the rigid silica scaffold allowing for a sufficient thermal treatment to be performed. In some cases, high temperature treatments are necessary to increase the degree of crystallinity, form a specific crystalline phase, graphitize or increase the stability of the materials. Such high temperatures can easily be applied during the nanocasting procedure thus enabling the synthesis of crystalline products without losing the mesostructure ordering; the rigid matrix skeleton preventing the collapse of the pore system [7–22].

Regarding the synthesis of nanocast mesostructured oxide compositions, most of the studies have focused on single metal oxides. On the other hand, mixed metal oxide compositions which contain two or more metallic elements in their lattice remained rare, although mixed compositions put forward several advantages in comparison to oxides of individual metal components [30–34]. These materials can be obtained either by doping a small amount of a second metal component on the lattice of a metal oxide, or as well-defined structures with mixed stoichiometry, e.g., spinels or perovskites. The most important advantage of such multi-component systems is that interactions between these active components can lead to new or improved properties, which will influence catalytic activity, selectivity, stability, etc. Cooperative synergetic effects which can arise from the intimate

combination of different metals coupled with nanostructure effects, such as high surface area and controlled pore structure, could lead to interesting new materials for advanced catalytic applications.

In the following, we will discuss some of the recent developments regarding the synthesis of nanocast mixed metal oxides and their perspectives for catalytic applications. In particular, series of advances were achieved in the recent years from our side regarding the development of mixed metallic oxide compositions with high surface area, and their prospects for industrially relevant catalytic processes [35–39]. It is here the choice of the authors to place emphasis on a few representative examples of compositions (e.g., non-noble metal-based catalysts, perovskites) and catalytic reactions (e.g., hydrogen production, oxidation). A concise review of these efforts is presented in this account.

2. General principles for the synthesis of nanocast (mixed) metal oxides

As indicated above, hard-templating process is a powerful method to create non-siliceous mesoporous materials that are difficult to synthesize by processes utilizing cooperative assembly between surfactants (e.g., ionic alkylammonium halides, or non-ionic block copolymers) and inorganic species [16–22]. Rigid templates may be very diverse, but a relatively general procedure for nano-replication can be given (see scheme in Fig. 1). In the first step of a structure replication process, the pores of the matrix are filled with the precursor for the desired product, for example, metal salts such as nitrates for metal oxides. This is usually realized by impregnation with a precursor solution, either by a "wet impregnation" or by the "incipient wetness" technique. The interaction of the precursor species with the pore walls is crucial, and it may involve hydrogen bonding, coordination of metal ions (e.g., on silanol groups), Coulomb interactions, and van der Waals forces, which facilitate the migration of metal ions. Other approaches to efficiently infiltrate the precursor species into the pores of the matrix include vapor-phase infiltration and infiltration in the liquid/molten state in absence of solvent. After the infiltration of the precursors and, if needed, the subsequent removal of the solvent, the formation of the wanted product is typically accomplished at elevated temperatures. In short, this synthetic pathway involves four main steps as illustrated schematically in Fig. 1: (1) choosing and generating the original template (mesoporous silica or carbon are usually used), (2) filling the mesopores with the precursors of the target composition, (3) converting these precursors into a continuous solid (*i.e.*, formation of a composite consisting of the original template and a target inorganic/polymeric solid), and finally, (4) removing selectively the original template by a chemical or a thermal treatment. The great advantage of this approach is the possibility of replication of complex mesophases and mesopore topologies with a precise level of structural and compositional control. Furthermore, morphology and particle shape of the template may be conserved for the nanocast replicas (e.g., spheres, thin films, monoliths [40–43]).

The target material is usually not incorporated in the pore system of the template as such, but under the form of a precursor (often in solution) that has to be converted subsequently into the final material. This precursor needs to meet several requirements: first, as it must enter the template structure, it must either be gaseous, highly soluble, or liquid at moderate conditions, so that it can be infiltrated into the voids of the template while achieving high loadings [9,44–48]; second, conversion to the desired composition should be simple and with as little volume shrinkage as possible; and finally, in most of the cases, it should not react chemically with the solid template. Metal nitrate salts are attractive precursors due to their high solubility, and availability at low cost. Moreover, pure oxides can be obtained because of the facile and complete removal of nitrates via thermal decomposition. Then, when choosing the original template, two important points must be considered. One is whether the template can maintain its ordered mesostructure during the conversion process in the third step. The other is whether the template can be easily removed without disrupting the mesoporous structure in the resulting replica. One of the most versatile hard templates is ordered mesoporous silica, since it can be prepared in diverse pore structures and morphologies [49]. Note that, these silica materials dissolve rather easily in HF or concentrated NaOH solutions, but multiple treatments are often needed to ensure optimal removal of silica. Though, it is not unusual to detect residual silicon (a few %) in the nanocast oxides when silica is removed using NaOH.

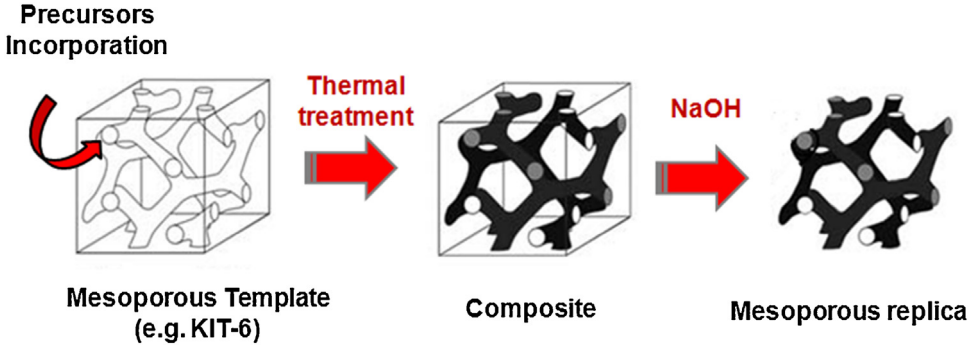

Fig. 1. Schematic representation of the nanocasting synthesis using mesoporous silica KIT-6 as the solid template.

The infiltration of the precursor into the pore channels is one of the most important factors in nanocasting. The so-called wet impregnation technique is commonly used [9,46,48], in which the solid template is dispersed in a dilute solution of precursors in order for the solute species to migrate and to be adsorbed on the pore surface upon solvent evaporation. This method often results in low level of loading of the pores with the precursors. Another widely used technique is the dry impregnation, also called incipient wetness [47,50,51]. In this method, a saturated solution of the precursors is used and the volume of the solution is restricted to the pore volume of the hard template used. Although the incipient wetness technique usually leads to a higher precursor loading, multiple impregnation steps are often required for optimized filling of the pores. Alternatively, a solid-liquid route, which is based on using molten nitrate salts for infiltrating the mesoporous silica without of the need of a solvent, has been applied to increase oxide loadings in the mesoporous host [52,53]. In all these cases, however, the unique driving force for accelerating the movement of the precursor solution into the mesopore channels is capillary effects. Therefore, improving capillary force could facilitate the migration of the precursor species. Generally, the metal precursors used in nanocasting are hydrophilic. It is believed that enhancing the hydrophilic character of the pore walls can increase the incorporation of the precursor with a high filling degree. For this purpose, surface functionalization of mesoporous silicas by certain organic groups (e.g., $-NH_2$, $-CH{=}CH_2$) was attempted in order to improve the interaction between the pore walls of the template and the metal precursors [51,54,55]. Another way is to maintain a high surface silanol concentration by performing acidic solvent extraction or oxidation under microwave conditions to remove the structure-directing agents used in the synthesis of the parent mesoporous silica template, instead of calcination at high temperature [9,17,45,46]. These above strategies can indeed improve the interactions between the pore walls of the template and the precursors through hydrogen and/or coordination bonding. However, these surface interactions are in fact mostly effective for the first layer of adsorbed precursor species. As the amount of precursor loading needed to obtain a mesostructure replica is far higher than the amount of a monolayer adsorption, the interactions between the precursors themselves are therefore also critical to reach high loading. In addition, too strong interactions between precursors and pore surfaces may hinder the migration of the precursors throughout the structure and, consequently, block the channels.

Beside these chemical aspects, the physical aspects should not be underestimated in the infiltration process. The impregnation process may be viewed as the replacement of a solid-gas interface by a solid–liquid interface [44]. Here, the pressure developed in the nanopores upon impregnation caused by compressed air bubbles may reach several MPa depending on the liquid–gas interfacial tension and the pore size of the mesoporous template. The higher the surface tension of the precursor solution and smaller the size of the template selected, the higher is the pressure in the air bubbles inside the pores [44,56]. The development of high pressure could impose large forces on the portions of the pore walls in contact with these bubbles, which may degrade the mesopore framework of the support upon impregnation. Moreover, replacement of the solid-gas interface by a solid-liquid interface generally causes a substantial heat release which may alter the quality of impregnation when using high concentration of precursors. Some methods for preventing or limiting the degradation of the mesoporous template can be employed, such as operating impregnation under vacuum, using fairly volatile solvents (alcohols or acetone are widely used in nanocasting), or adding a surfactant to the solution. However, these solutions either are difficult for practical application or lead to a lower precursor filling because of the presence of additives or the use of less polar solvents (*i.e.*, lower solubility of metal precursors in the solution). One interesting alternative method called the "bi-solvent technique" was proposed to overcome precursor infiltration issues [28,57]. In the method, the support is first dispersed in a pure less wetting solvent prior to being placed in the impregnation solution. Here, the characteristics of exothermic effects and high pressure development are no longer valid in the step of impregnation. The driving force for the infiltration of the metal precursors into the pore channels is a concentration gradient. In connection to that, our group recently developed a versatile one-step-impregnation synthesis method, which was shown particularly suitable for preparation of nanocast mixed metal oxide compositions using nitrate salts as precursors [35]. This method is based on using molten nitrate salts in the presence of an organic solvent (e.g., *n*-hexane or cyclohexane) under refluxing conditions, to infiltrate different mesoporous silicas used as typical solid templates. In the conventional solid-molten liquid method described above, the molten metal salts are highly viscous with high surface tension, which could limit diffusion in the mesopores and thus induce high pressure during the infiltration process. Such drawbacks of directly using molten metal salts can be overcome if the pore space of the silica support is first filled with alkane solvents, which have much lower surface tension than highly concentrated salt solutions, prior to being placed in contact with the metal precursors. This method was implemented with success to a variety of mixed oxides (see below) [35].

After the impregnation step, subsequent drying and thermal treatment(s) to convert the precursor into the desired metal oxide are also important steps in the course of the replication process. Here, diffusion, nucleation, particle growth and phase transformations take place during drying and thermal treatments. In mixed oxide systems, the uniformity of the replicated composite may be influenced by the choice of metal precursors, and the presence of chelating agents (e.g., citric acid, glycine) may be needed to achieve homogeneous precursor distribution as it is, for instance, the case for the nanocast synthesis of perovskites. In turn, the physical and chemical properties of resulting material can be linked to several parameters inherent to the treatment conditions used. For example, the size of the replica particles was shown to be strongly affected by the environment atmosphere during thermal treatment [58]. In fact, the impact of drying and thermal

treatment on the structural and catalytic properties of conventional supported catalysts is well documented [49–61], yet much of the literature on nanocast materials has not considered these aspects.

In comparison to single metal oxides, much fewer studies were performed regarding the synthesis of nanocasting mixed metal oxides (Table 1). The first nanocasting syntheses of mesoporous mixed oxides were reported by Schwickardi et al. [62] who described the preparation of phase pure spinels ($ZnCr_2O_4$, $CoCr_2O_4$, and $NiAl_2O_4$) and $LaFeO_3$ perovskites, which exhibited disordered pore structure, using activated carbon as a solid template and various metal nitrates as the precursors. These materials were found to possess much higher values of specific surface area in comparison to their bulk counterparts. Later in 2005, Valdés-Solis et al. reported the synthesis of high surface area spinels and perovskites, this time using porous silica xerogel as a template [63]. Following these early efforts, Sun et al. reported single phase mesoporous $CoFe_2O_4$ through nanocasting of SBA-15 and KIT-6 templates with nitrate precursors [64]. These spinels possessed high degree of crystallinity and large specific surface areas ($> 130\ m^2\ g^{-1}$). Their highly ordered mesoporous structure was confirmed from transmission electron microscopy (TEM) images, electron diffraction and low angle X-ray diffraction (XRD) patterns. Ordered mesoporous $NiFe_2O_4$ with excellent microwave absorption properties was also synthesized by using mesoporous silica (KIT-6) as a template [50]. The periodic mesostructure was here confirmed by TEM, high-resolution scanning electron microscopy (HR-SEM) (Fig. 2) and low angle XRD. Here, it is worth mentioning that, HR-SEM has become a really powerful technique to study the mesostructure of nanocast metal oxides [65–67].

Using our one-step-impregnation nanocasting method, we synthesized high surface area mixed metal oxides (e.g., $NiFe_2O_4$, $CuFe_2O_4$, Cu/CeO_2), which are quite difficult to prepare otherwise [35]. For these structures, SBA-15, KIT-6 silicas and MCM-48 silica nanospheres were chosen as the solid templates. Representative TEM images and N_2 sorption isotherms, with the corresponding pore size distributions, of the obtained materials are shown in Figs. 3 and 4, respectively. Interestingly, the use of MCM-48 silica nanospheres (particles ~150 nm) demonstrated very nicely the ability of retaining the particle morphology into the nanocast oxide replica. As another example, a series of nanocast mesoporous perovskites was synthesized by Nair et al. using ordered mesoporous KIT-6 silica as the hard template. The perovskites were prepared with lanthanum in the A site and manganese, cobalt or iron in the B site of the ABO_3 structure [37]. In this case, a citrate complex made using the metals in the appropriate stoichiometry was impregnated into the template pores by the method of wet impregnation.

Despite a great number of contributions dealing with nanocasting syntheses, the number of articles discussing applications of the nanocast materials, particularly in catalysis, still remains far behind. However, studies on surface redox reactivity, confinement of reactions near to the surface owing to the dimension of the pores, and synergistic interaction between catalytic components in nanocast mixed metal oxides are certainly valuable to develop and produce new efficient catalysts [11,20,21,68–70]. Some examples will be discussed in the following.

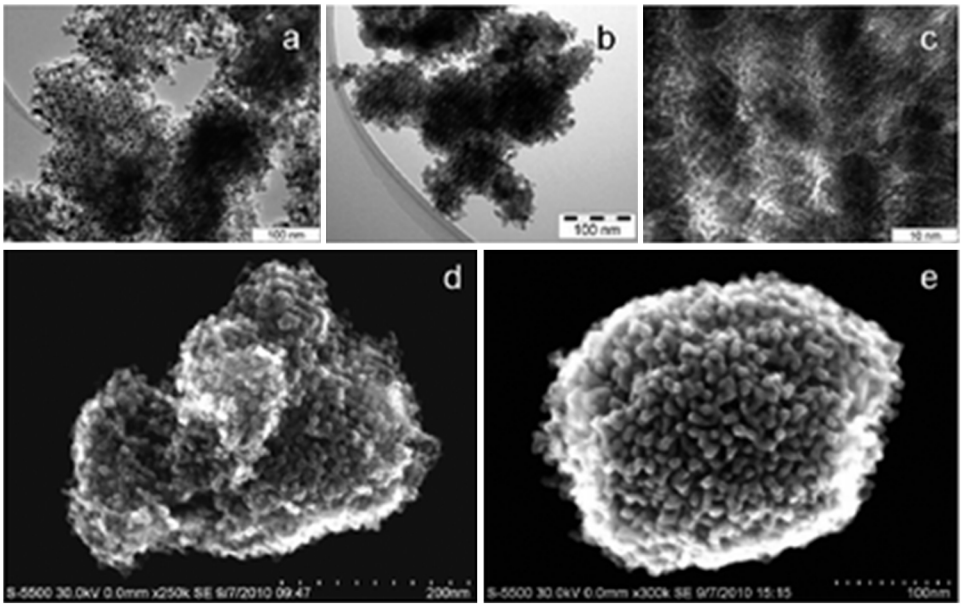

Fig. 2. Transmission electron microscopy (TEM) images (a, b and c) and high-resolution scanning electron microscopy (HR-SEM) images (d and e) of meso-$NiFe_2O_4$.
Reprinted with permission from reference [50]. Copyright 2011 (RSC).

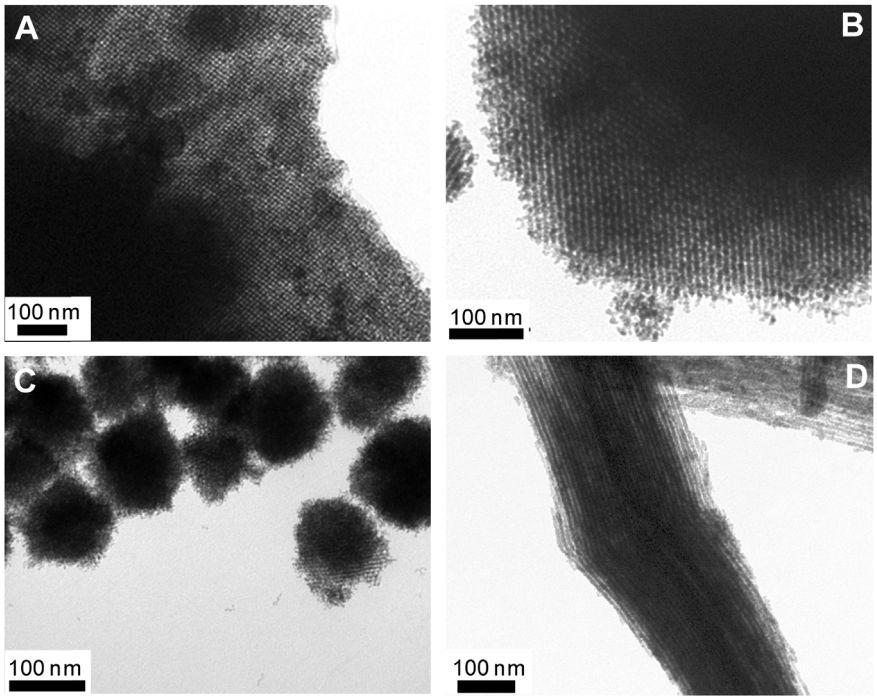

Fig. 3. Representative TEM images of the nanocast mixed oxides prepared from different mesoporous silica templates: (A) Cu(30)Ce-K100, (B) Cu(30)Co(20)Ce-K100, (C) Cu(30)Ce-MCM and (D) Cu(30)Ce-SBA.
Reprinted with permission from reference [36]. Copyright 2012 (Wiley).

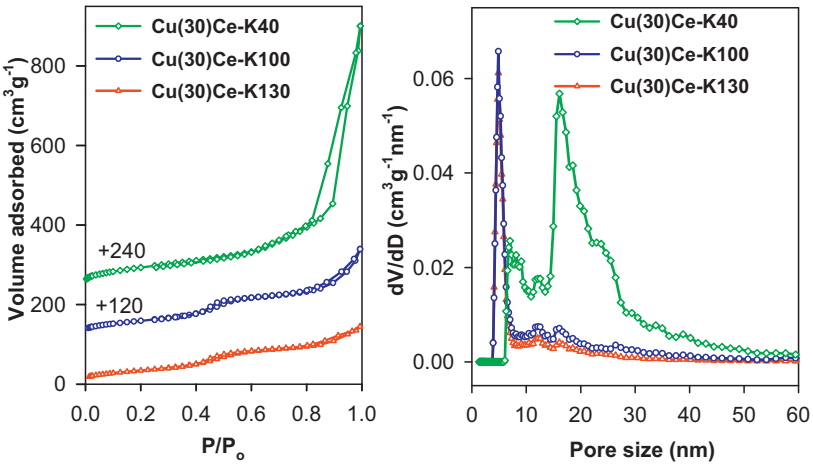

Fig. 4. (Colour on line.) N_2 adsorption-desorption isotherms at −196 °C (left) and respective NLDFT pore size distributions (right), deduced from the adsorption branch for the nanocast Cu/CeO_2 mixed metal oxides.
Reprinted with permission from reference [36]. Copyright 2012 (Wiley).

3. Examples of catalytic applications of nanocast mixed metal oxides

3.1. Copper/ceria-based catalysts (preferential oxidation of CO)

Hydrogen is considered as the most efficient and clean energy source for fuel cells. H_2 is produced mainly by reforming of hydrocarbons, followed by the water gas shift reaction, which leads to the presence of CO as an impurity that must be removed. Low temperature oxidation of this CO (0.5–2%) is thus inevitable as part of the purification of hydrogen to feed proton-exchange membrane fuel cells (PEMFCs) [68,71–73]. The most attractive catalysts for the preferential oxidation (PROX) of CO in excess H_2 are gold-based materials [74,75]. Co_3O_4-based systems also gained some attention as cost-effective alternatives [76–78]. However, although CO conversion was reported to reach

100% at ambient temperature using Co_3O_4 for a gas mixture consisting of 0.5% CO, 14.4% O_2 and 85.1% N_2 with a space velocity of 4000 mL g_{cat}^{-1} h^{-1}, severe deactivation was observed [78].

In fact, regarding catalytic oxidation, CO oxidation is one of the most studied reactions using nanocast catalysts. For example, Shen et al. synthesized mesoporous CeO_2 with well-developed 3-D cubic ordered pore structure (confirmed by TEM images and low angle XRD) using KIT-6 as the solid template [79]. FE-SEM images showed that the size of the nanocast ceria particles were below 100 nm, and only traces of Si remaining after removal of the template were detected by elemental analysis (EDS). These materials exhibiting a specific surface area of 112 m^2 g^{-1} showed excellent CO conversion efficiency in comparison to CeO_2 catalysts synthesized by the conventional decomposition method. These authors also showed that by loading 20% of CuO on these nanocast CeO_2 replicas, T_{50} (the temperature required to attain 50% conversion for the reaction) could be decreased down to 115 °C [79]. Among several other nanocast oxides studied for CO oxidation, Co_3O_4, β-MnO_2 and NiO synthesized from KIT-6 showed high conversion even below 0 °C [68], whereas mesoporous Fe_2O_3 was the least active. Here, the catalytic activity of these materials was found to depend on the pre-treatment temperature applied. Before that, Tüyüz et al. [11] had already synthesized mesoporous Co_3O_4 as a CO oxidation catalyst with enhanced specific surface area, also using KIT-6 silica as the hard template. They observed 100% conversion of CO to CO_2 around room temperature at a space velocity of 18,000 mL g_{cat}^{-1} s^{-1}. The activity was correlated to the textural properties of the catalysts, in which that with the highest specific surface area and the most open pore structure was found to be the most active. However, about 50% loss of activity was observed over 4 h during the course of the reaction.

Nanocast mixed oxides, e.g., $CuCo_2O_4$, $MnCo_2O_4$ and $NiFe_2O_4$, synthesized from SBA-15 were also tested for CO oxidation. Among these materials, $CuCo_2O_4$ and $MnCo_2O_4$ demonstrated high activity and good stability, whereas in the case of $NiFe_2O_4$ a continuous deactivation was observed [80].

Among various compositions, copper/ceria-based catalysts are considered as some of the most promising candidates for the PROX process because of their low cost and high selectivity for CO [81–85]. However, they usually only show noticeable catalytic activity above 100 °C, while the operating temperature of PEMFC is around 80 °C. Furthermore, the catalytic properties of these materials were found to depend strongly on the preparation method and the resulting CuO/CeO_2 interfacial area [83–85]. Thus, we investigated the catalytic performance of nanocast Cu/

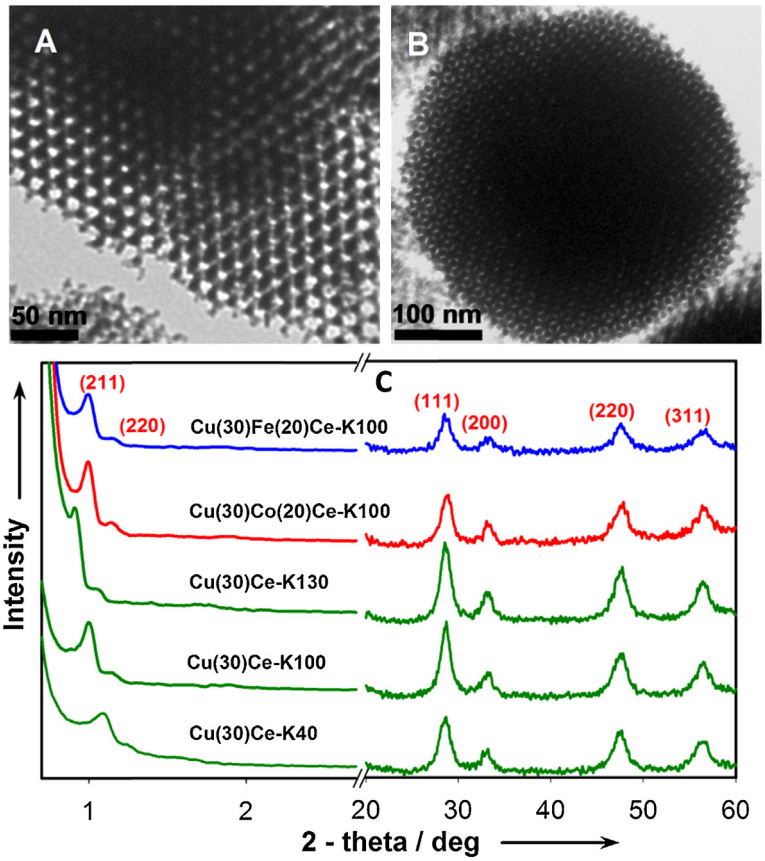

Fig. 5. (Colour on line.) TEM images Cu(30)Ce-K40 (A) and Cu(30)Fe(20)Ce-K100 (B); Powder XRD patterns of the samples templated from KIT-6 (C). Reprinted with permission from reference [36]. Copyright 2012 (Wiley).

CeO_2 and CuM/CeO_2 (M = Fe and Co) mixed oxides for their effectiveness in the CO-PROX [36]. The catalysts were synthesized by the one-step-impregnation nanocasting method [35]. Fig. 5A and B show representative TEM images of the nanocast materials replicated from KIT-6 and SBA-15 templates, confirming the long-range periodic order of the mesopores. The excellent mesostructure order of the mesoporous metal oxides was also demonstrated by low angle XRD patterns (Fig. 5C). All the XRD patterns exhibit a main strong peak at low 2-theta value, which can be indexed to the (211) and (100) reflections of the *Ia*3*d* and *p*6*mm* symmetries, respectively. The crystalline nature of the walls of the mesoporous materials was confirmed by wide-angle XRD analysis (Fig. 5C), which reveals peaks corresponding to the pure face-centered-cubic (fcc) structure of CeO_2. The absence of other oxide phases of copper, cobalt or iron suggests that these metal species are highly dispersed or incorporated in the ceria lattice. Here, the remaining Si content determined by atomic absorption spectroscopy (AAS) was about 3.5 wt% in all samples. The corresponding activity and selectivity for CO-PROX of all the samples, plotted as function of temperature, are shown in Fig. 6. The catalytic performance of these materials was among the best reported for copper/ceria-based compositions both with respect to the CO conversion and CO_2 selectivity at low temperature. A complete CO conversion with 100% selectivity was achieved at around 40 °C in the case of Cu/CeO_2 synthesized using KIT-6 silica aged at 40 °C, where the amount of Cu was 30 molar %. Interestingly, negligible decline was observed for the performance of these materials even after three cycles of operation. Furthermore, it was observed that the incorporation of 20% Fe extends the full CO conversion range (80–160 °C) with an enhanced selectivity to CO_2, while Co incorporation does not provide substantial improvement.

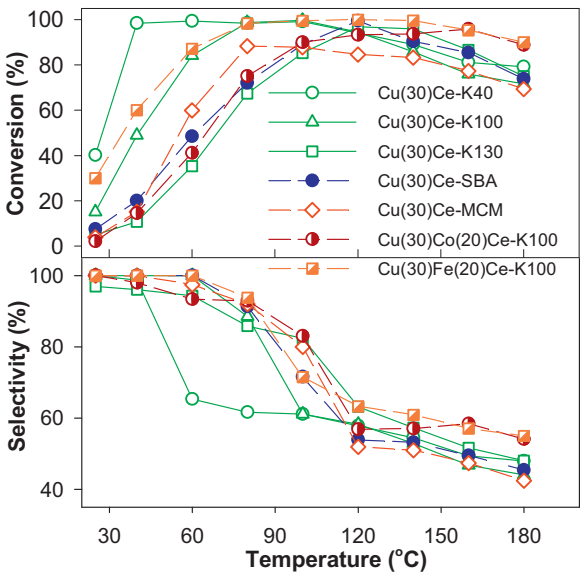

Fig. 6. (Colour on line.) Conversion and selectivity as a function of temperature for CO-PROX over nanocast Cu/CeO_2 and CuM/CeO_2 catalysts (1.64% CO, 1.62% O_2, 90.25% H_2, balance He, space velocity: 37 L h^{-1} g^{-1}). Reprinted with permission from reference [36]. Copyright 2012 (Wiley).

However, further studies will be needed to clarify the impact of the Fe and Co doping. Moreover, the light-off temperatures of CO (T_{50}) was found in this study to strongly depend on variations in oxygen vacancies and reducibility. In addition, indications regarding the influence of structural parameters, such as pore size and pore structure, on the reducibility and catalytic properties were also found.

It was proven previously for single mesoporous oxides used in CO oxidation that, the high specific surface area of the nanocast metal oxides was not the only reason for their high activity; the type of mesostructure being important as well. In the case of single oxide Co_3O_4, Tüyüz et al. [11] showed clearly that the light-off temperature of CO (T_{50}) increased with the decreasing surface area of nanocast Co_3O_4. However, from the slope of the conversion curve obtained for a Co_3O_4 catalyst prepared from KIT-6 aged at the highest temperature (135 °C), the authors suggested that it could indicate the occurrence of pore diffusion limitation effects in this narrow pore system (3 nm in pore size). This idea was supported by the fact that the catalytic activity normalized to specific BET surface area was not constant. The normalized catalytic activity was actually the highest for Co_3O_4 prepared from KIT-6 silica aged at 40 °C (i.e., the most open Co_3O_4 pore system). This particular catalyst with an uncoupled sub-framework structure showed very high activity for CO oxidation at low temperature, which was comparable to very good gold-based catalysts. In this system, full CO conversion was reached at room temperature over the Co_3O_4 nanocast catalyst possessing a specific surface area of 153 m^2/g and pore size of 6 nm. Whereas, the Co_3O_4 sample having a specific surface area by just a factor of two lower (70 m^2 g^{-1}) showed almost no conversion at this temperature. Obviously, in the case of mixed oxide mesoporous materials, such mesostructure effects can also be expected. However, in addition to specific surface area and mesostructure, the catalytic activity per surface active site and the selectivity can also depend strongly on metal-support interactions (e.g., one of the metals acts as active site and the other is more serving as a support matrix). Therefore, here, the catalytic activity of the catalyst should in fact be normalized to surface area of active sites. However, determination of active sites is a complicated task and it frequently remains elusive. In addition, there is often a complex interplay between textural and chemical properties which makes rather difficult a precise distinction between the impacts of each parameter on the catalytic reactivity.

3.2. Copper/nickel-based catalysts (H_2 production)

In terms of clean energy, H_2 is viewed as the best alternative to hydrocarbon fuels due to its high energy content and its environmentally-benign impact. However, for practical use, it is necessary to store hydrogen safely, reversibly, and at high gravimetric/volumetric capacity. Among the possible solutions, one of the promising hydrogen storage techniques relies on liquid-phase chemical storage materials, e.g., ammonia borane, hydrazine and formic acid [86,87]. Ammonia borane (H_3N–BH_3,

AB) is a particularly appealing molecule for chemical hydrogen storage applications owing to its high gravimetric capacity of H_2 (theoretical 19.6 wt%), good stability and solubility in relatively polar coordinating solvents under ambient conditions. Catalytic hydrolysis, which can in theory produce 3 mol of H_2 per mole of AB (equation (1)), is an effective approach for the release of H_2 stored in AB [88,89].

$$H_3NBH_3 + 2H_2O \rightarrow NH_4^+ + BO_2^- + 3H_2 \quad (1)$$

Initially, rapid hydrogen generation was achieved using noble metal catalysts (such as Pt, Ru, and Rh). Now, finding cheaper, highly efficient and selective catalysts for these reactions is important [90–92]. Regarding the cheaper transition metal alternatives, instability of their low valence active states for hydrolysis of AB is a major issue [93–95]. Studies performed using supported non-noble metals indicated some activity for Co, Ni and Cu, whereas Fe is catalytically inactive for this reaction [96]. Among the different supports studied (Al_2O_3, SiO_2 and C) for Co nanoparticles, the Co/C catalyst was found to show the highest activity. However for such transition metal catalysts, reductive pre-treatment and/or the use of protective agents were unavoidable. Nevertheless, this may be overcome by using an oxide from which a metallic catalyst is formed under mild reductive reaction conditions. In connection to that, copper oxides were reported to be operating in AB hydrolysis without the need for a reductive pre-treatment. In this case, however, pronounced agglomeration of Cu formed during the reaction decreased drastically the catalytic activity [94,95].

Besides, bimetallic catalysts usually show enhanced catalytic performance in comparison to their monometallic counterparts. In studies performed using Pt/Ni catalysts, $Pt_{0.65}Ni_{0.35}$ displays the highest catalytic performance with a high hydrogen release rate of 4784.7 mL min^{-1} g^{-1} and low activation energy of 39.0 kJ mol^{-1} [97]. A synergistic improvement of catalytic activity in AB hydrolysis reaction was also observed for Ni/Pt hollow bimetallic spheres [98]. Evidently, *cooperative* effects will play important role in accelerating H_2 evolution in such systems. Thus, there is an interest in developing an efficient catalytic system without noble metals, while at the same time using similar synergistic effect. To this aim, we recently reported the excellent catalytic performance of bi-component nanocast CuO–NiO catalysts for the AB hydrolysis [38]. The performance of these CuO–NiO materials toward the catalytic hydrolysis of AB was evaluated on the basis of the amount of H_2 gas released. Our studies showed that interactions existing between Cu species and NiO, in comparison to pure CuO and NiO, have an strong influence on accelerating the hydrogen evolution of AB. Fast completion of hydrolysis was achieved in the case of nanocast Cu/Ni-based catalysts (2 min) with an initial turnover frequency (TOF) value of 3600 h^{-1} (mol of H_2 per mol of Cu per hour) under ambient conditions, which is the highest value reported thus far among all the non-noble metal catalysts for this reaction. The sample that contained an equal ratio of Cu and Ni was found to be the most active catalyst. Also, the calcination temperature of the samples was found to have an influence on the catalytic activity (400 °C being the best temperature here). Considering the poor catalytic performance of the individual components (Ni or Cu), a synergetic interaction between copper and nickel in solid solution seems indeed to be the key towards the enhancement of the catalytic activity in the AB hydrolysis. Further evidence for synergistic interactions between the metals, thereby enhancing the reducibility of both Cu and Ni species, were derived from the TPR-H_2 profiles (Fig. 7). The lower onset temperature of reduction for the bulk $Cu_{0.5}Ni_{0.5}$ oxides compared to that of individual CuO and NiO confirmed the presence of interactions between Cu and Ni. Interestingly, the onset of reduction and the completion of this process occurred 25 °C and 85 °C lower, respectively, for the nanocast sample in comparison to a similar bulk composition. In this comprehensive study, kinetic parameters of AB hydrolysis were monitored both for nanocast and bulk CuNi (1:1 ratio) catalysts. The reaction rate was found to be first order with respect to the catalyst concentration. The apparent activation energies for hydrolytic dehydrogenation were estimated to be 39 and 42 kJ mol^{-1} for the nanocast and bulk catalyst, respectively, indicating that the greater population of active sites in the nanocast catalyst resulted in the distinctively higher activity of this material compared to the bulk equivalent (Fig. 8). This study clearly showed that metal precursors, composition, and heat treatment conditions have a profound influence on synergetic interactions existing between Cu species and NiO, which are decisive in accelerating the hydrogen evolution of AB. Such insights demonstrate that combinations of non-noble metal can provide viable solutions for the development of practical catalysts, first for H_2 generation from AB hydrolysis, but possibly also for other challenging reactions.

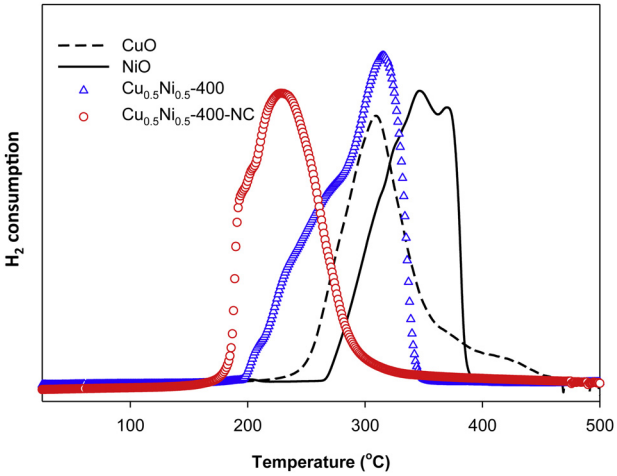

Fig. 7. (Colour on line.) H_2-TPR profiles of CuO, NiO and $Cu_{0.5}Ni_{0.5}$ samples. Reprinted with permission from reference [38]. Copyright 2013 (RSC).

As discussed above, in addition to specific surface area and structure, the catalytic activity per surface active site and the selectivity can depend strongly on metal-support interactions. For instance, in our study on the hydrolysis of ammonia borane, it was observed that the sample $Cu_{0.5}Ni_{0.5}$-600 possessed a surface copper content twice

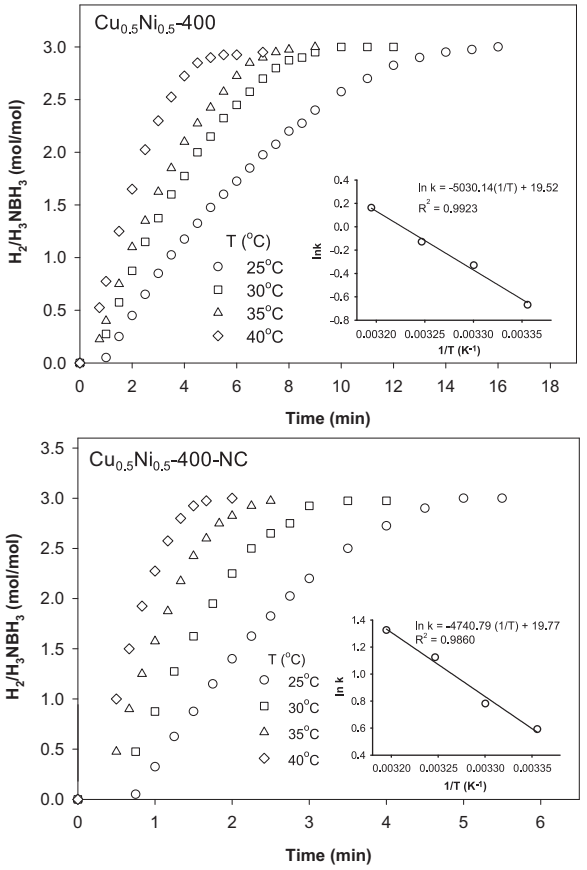

Fig. 8. Plots of the volume of generated H_2 vs. time over $Cu_{0.5}Ni_{0.5}$-400 and $Cu_{0.5}Ni_{0.5}$-400-NC catalysts at different temperatures ([Cu] = 3.2 mM, [AB] = 148 mM). (Inset: Arrhenius plot.) [38].
Reprinted with permission from reference [38]. Copyright 2013 (RSC).

higher than $Cu_{0.5}Ni_{0.5}$-400, while surface areas of these samples were rather comparable (7 and 10 $m^2 g^{-1}$, respectively). However, the reaction rate over $Cu_{0.5}Ni_{0.5}$-400 was still five times higher than that of $Cu_{0.5}Ni_{0.5}$-600 because the latter material consists of mainly individual oxide phases. Also, in an attempt to compare the reactivity of bulk and mesoporous $Cu_{0.5}Ni_{0.5}$, we found that the mesoporous sample exhibited a reaction rate three times higher than its bulk counterpart, while the surface area of the porous sample is seven times higher (73 $m^2 g^{-1}$ and 10 $m^2 g^{-1}$ for the porous and bulk materials, respectively). From this, it was deduced that metal (oxide) surface area alone cannot explain the differences in performance, because copper exists in different states (in NiO matrix support and in single CuO phase) that have distinct reactivities. In such cases, the activity of the catalyst may be normalized to the surface area of the active sites, if it is determined accurately.

3.3. Nanocast perovskites as oxidation catalysts

Another interesting class of mixed metal oxides are perovskites (ABO_3). For heterogeneous catalytic applications, these materials generally comprise of a lanthanide (La is the most common) in the A site and a transition metal (Mn, Co, Fe, etc.) in the B site. In addition, these materials can be synthesized by partially substituting either or both of the A and B sites. The efficiency of such perovskite oxides, either substituted or not, is well documented for a variety of catalytic applications [99–104]. Specifically, the importance of these materials lies in the fact that some studies established that the catalytic efficiency of these materials was comparable to that of noble metals in various reactions. Early on, Arai et al. revealed the efficiency of perovskite-type oxides for the total oxidation of methane and compared it with Pt/alumina catalyst [105]. Of the oxides examined by these authors, strontium-substituted $LaMnO_3$, was found to be superior to the Pt/alumina catalyst at a conversion level below 80%. More recently, Kim et al. studied the effect of Sr substitution in $LaCoO_3$ and $LaMnO_3$ perovskites for diesel oxidation (DOC) and lean NO_x trap (LNT) processes. These authors observed that the perovskites could efficiently outperform Pt-based catalysts in these reactions [106]. In particular, $La_{1-x}Sr_xCoO_3$ catalysts achieved higher NO to NO_2 conversions than the commercial Pt-based catalyst under realistic conditions. Also, the $La_{1-x}Sr_xMnO_3$ LNT catalyst showed NO_x reduction performance comparable to that of the commercial Pt-based counterpart.

However, a major challenge persisting in the commercialization of these perovskite materials is their inherent lower values of specific surface area resulting from the required high temperature of synthesis [104]. For this reason, one major objective regarding these materials was to produce them with enhanced values of specific surface area. Although several solid- and liquid-phase syntheses were developed, the values of surface area achieved still remained inferior to 30 $m^2 g^{-1}$. Studies regarding nanocast perovskites [62,63] and their catalytic applications are surprisingly rare. Wang et al. performed the first catalytic study on nanocast perovskites [107]. The efficiency of mesoporous $LaCoO_3$ was monitored for the total oxidation of methane and was compared with a bulk counterpart,

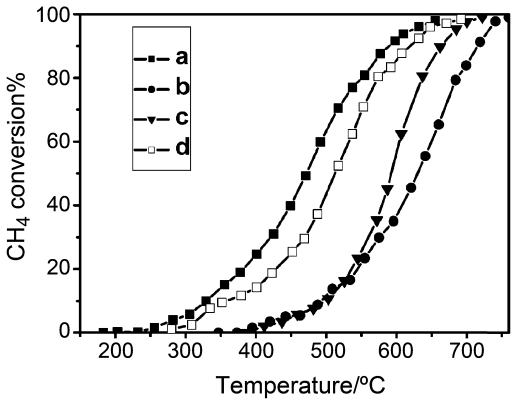

Fig. 9. Temperature dependence of methane combustion on (a) mesoporous $LaCoO_3$ after removal of silica, (b) mesoporous $LaCoO_3$/silica hybrid material and (c) conventional $LaCoO_3$ and (d) used mesoporous $LaCoO_3$ catalyst.
Reprinted with permission from reference [107]. Copyright 2008 (ACS).

which was synthesized using the citrate method (Fig. 9). The light-off temperature (defined here as $T_{10\%}$) and the half-conversion temperature (T_{50}) were at 335 and 470 °C, respectively, being much lower than those obtained in the case of bulk perovskite at a space velocity of 60,000 h^{-1}. However, when the catalytic run was performed for a second cycle, the activity slightly declined (but was still better than the conventional $LaCoO_3$). The authors also noticed a small decrease in specific surface area indicating that some degree of particle sintering occurred during the reaction. The redox properties and surface compositions, as analyzed by H_2-TPR and XPS techniques, indicated the presence of high valence cobalt ions and high content of O_2^{2-}/O^- species and these species were correlated to the high activity of these materials, besides the high specific surface area. Differently, de Lima et al. reported the repeated nanocasting preparation of mesoporous $LaFeO_3$ and $LaFeCoO_3$ perovskites using a porous carbon template [108], which was synthesized in a previous step using silica aerosil as a first solid template. These perovskites were studied for the reduction of NO to N_2 using CO as reducing agent, which itself is oxidized into CO_2 [108]. In the case of nanocast $LaFeO_3$, higher activity was observed for the reduction of NO to N_2 and oxidation of CO to CO_2 compared to the conventional $LaFeO_3$ obtained by the citrate method. The higher activity of the nanocast $LaFeO_3$ was attributed to a higher number of accessible active sites and hence the higher specific surface area. Nanocast $LaFeCoO_3$ also showed enhanced conversion; however in this case, performances were lower than the $LaFeO_3$ equivalent, owing to lower specific surface area of $LaFeCoO_3$ and the presence of binary oxide impurities observed on the wide-angle XRD pattern. Moreover, no deactivation of the nanocast catalysts was detected over 1400 min on stream at 380 °C.

In our laboratory, we performed the nanocasting synthesis of a series of mixed metal oxide perovskites with La in the A site and different transition metals (Mn, Co, and Fe) in the B site, using ordered mesoporous KIT-6 silica as the solid template [37]. For the synthesis, a citrate complex, prepared using the appropriate metal ratios, was carefully impregnated into the template mesopores using the wet impregnation method. After drying, high temperature (700 °C) calcination under air led to the formation

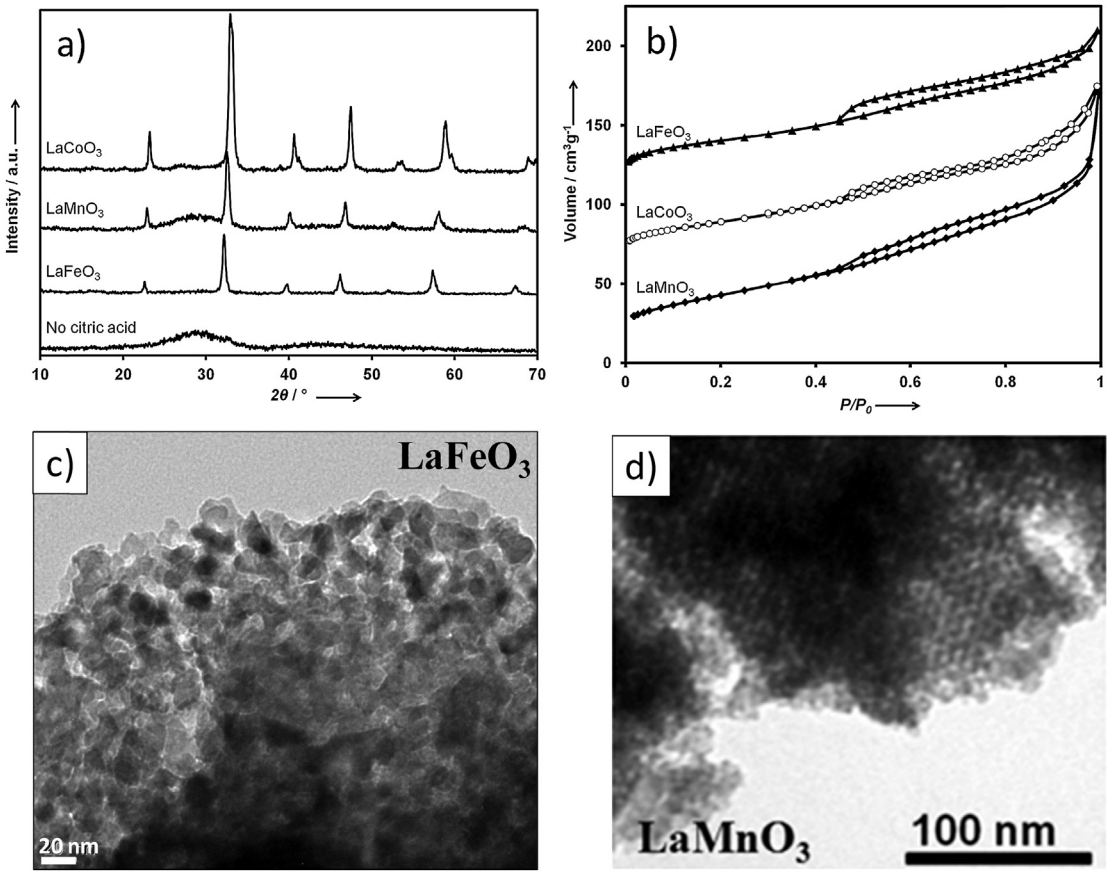

Fig. 10. a: wide-angle powder XRD patterns of mesoporous perovskite oxides synthesized using ordered mesoporous KIT-6 aged at 100 °C as the hard template. The lowest curve corresponds to the $LaMnO_3$ perovskite synthesized without using citric acid; b: N_2 physisorption isotherms of nanocast perovskite oxides synthesized using ordered mesoporous KIT-6 silica aged at 100 °C as hard template. The isotherms of $LaCoO_3$ and $LaFeO_3$ are plotted with an offset of 60 $cm^3\ g^{-1}$, and 110 $cm^3\ g^{-1}$, respectively, for clarity; c: TEM images of nanocast $LaFeO_3$ synthesized by use of ordered mesoporous silica as a hard template; d: TEM images of nanocast $LaMnO_3$ synthesized by use of mesoporous KIT-6 silica.
Reprinted with permission from reference [37]. Copyright 2012 (Wiley).

Table 1
Physicochemical parameters of the nanocast mixed metal oxides obtained from N_2 physisorption analysis at −196 °C.

Sample	Template	S_{BET} ($m^2\ g^{-1}$)[a]	D_p (nm)[b]	V_p ($cm^3\ g^{-1}$)[c]	References
$ZnCr_2O_4$	Activated carbon	72	–	–	[62]
$CoCr_2O_4$	Activated carbon	126	–	–	[62]
$NiAl_2O_4$	Activated carbon	165	–	–	[62]
$CoFe_2O_4$	SBA-15	155	9	0.35	[64]
$CoFe_2O_4$	KIT-6	129	11.7	0.37	[64]
$NiFe_2O_4$	KIT-6	121	3.6	0.27	[50]
$CuCo_2O_4$	SBA-15	99	5.4	0.41	[80]
$MnCo_2O_4$	SBA-15	129	5.4	0.35	[80]
$NiCo_2O_4$	SBA-15	91	5.3	0.35	[80]
$Cu(30\%)/CeO_2$	KIT-6	197	7/12	0.90	[36]
$Cu(30\%)/CeO_2$	KIT-6	146	4.9	0.30	[36]
$Cu(30\%)/CeO_2$	KIT-6	126	4.9	0.21	[36]
$Cu30\%–Fe20\%\ CeO_2$	KIT-6	153	4.9	0.26	[36]
$Cu30\%–Co20\%\ CeO_2$	KIT-6	162	4.9	0.24	[36]

[a] Calculated by using the BET method (0.05–0.2).
[b] Pore size.
[c] Pore volume.

of a perovskite-silica composite. Multiple impregnation-calcination cycles were needed in order to enhance the oxide loading. Subsequently, removal of silica by treating the powders with aqueous NaOH solution resulted in the formation of the mesoporous perovskites. However, although well-ordered mesostructure domains were clearly visible, less defined and disordered nanoporous regions were also present in these materials irrespective of the composition or the template used (Fig. 10). Crystallinity and phase purity of these nanocast perovskites were confirmed by wide-angle XRD analyses (Fig. 10a) [37,39]. Characteristic peaks corresponding to the perovskite structure were observed in the XRD patterns for all of the three compositions when citric acid is used. Without citric acid, an X-ray amorphous material was obtained. In addition, a low intensity broad peak (centred at $2\theta = 28^\circ$) was observed in the case of $LaMnO_3$, which points to the presence of residual X-ray amorphous Si species. Our studies indicated that the residual Si resulted from the formation of amorphous rare earth silicates [39]. Interestingly, the amount of these rare earth silicates varied with respect to the perovskite composition with the highest amount observed for $LaMnO_3$ [37]. In these samples, atomic absorption analysis revealed the presence of 3% Si in the case of $LaFeO_3$ and $LaCoO_3$, whereas for $LaMnO_3$ this amount was found to be as high as ~10%. The N_2 physisorption isotherms at −196 °C of these nanocast $LaMnO_3$, $LaCoO_3$ and $LaFeO_3$ perovskites demonstrate a type-IV behavior (Fig. 10b). An hysteresis loop appears in the relative pressure range from 0.5 to 1.0, which is rather typical of such mesoporous metal oxides obtained from nanocasting [9,10,13,36]. Specific BET surface areas obtained for nanocast perovskites are exceptionally high (up to 155 $m^2\ g^{-1}$) compared to those of materials obtained from conventional methods, especially considering the high calcination temperature of 700 °C (Tables 1 and 2).

The catalytic oxidation efficiency of these nanocast mesoporous perovskites was examined in the case of total oxidation of methanol as a model reaction. From the steady state conversion profiles, the nanocast mesoporous $LaMnO_3$ catalysts were found to show the highest conversion for methanol in comparison to both $LaCoO_3$ and $LaFeO_3$ nanocasts and $LaMnO_3$ samples prepared by other methods (Fig. 11) [37]. CO_2 was the only product detected, without any presence of formaldehyde or CO, which is another indication of the efficiency of these catalysts. Interestingly, some conversion, although rather low, was already observed near to room temperature for nanocast $LaMnO_3$. To obtain more insights into the reactivity of such nanocast oxides, kinetic data processing was performed for the total oxidation of methanol with the

Table 2
Physicochemical parameters of the nanocast perovskites obtained from N_2 physisorption analysis at −196 °C.

Sample	Template	S_{BET} ($m^2\ g^{-1}$)[a]	D_p (nm)[b]	V_p ($cm^3\ g^{-1}$)[c]	References
$LaFeO_3$	Activated carbon	49	–	–	[62]
$LaFeO_3$	Silica xerogel	110	–	–	[63]
$LaMnO_3$		41	–	–	
$LaCoO_3$	Vinyl-KIT-6	96	6	–	[107]
$LaFeO_3$	Carbon	49	–	0.07	[108]
$LaFeCoO_3$		30	–	0.09	
$LaMnO_3$	KIT-6	155	4.8	0.2	[37]
$LaCoO_3$	KIT-6	125	4.8	0.1	[37]
$LaFeO_3$	KIT-6	110	4.8	0.1	[37]

[a] Calculated by using the BET method (0.05–0.2).
[b] Pore size.
[c] Pore volume.

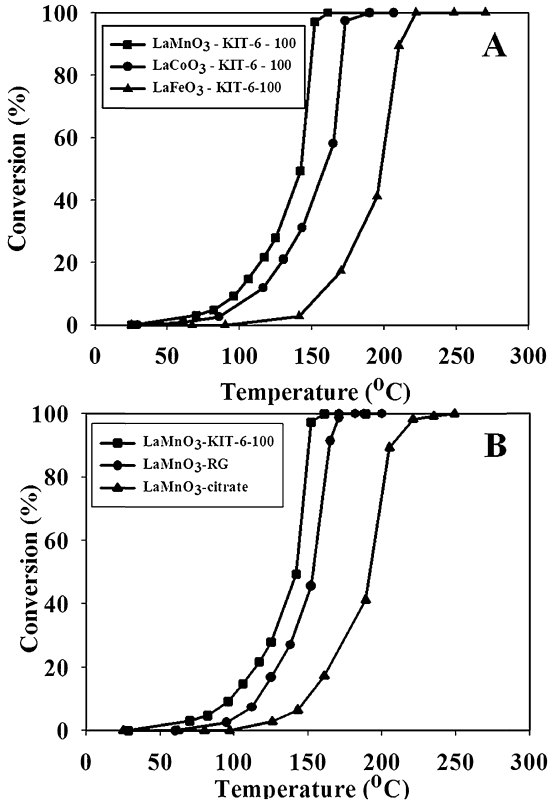

Fig. 11. Methanol conversion profiles as a function of temperature for: (A) a comparison between nanocast $LaMnO_3$, $LaCoO_3$ and $LaFeO_3$, and (B) a comparison between nanocast $LaMnO_3$ synthesized using KIT-6 aged at 100 °C and with the same composition synthesized by other methods. Reprinted with permission from reference [37]. Copyright 2012 (Wiley).

$LaMnO_3$ catalyst. For this purpose, temperature-dependent conversions were obtained at different flow rates [37]. The values of conversions at selected temperatures were then cross-plotted against pseudo-contact time, to generate the rate values. The results indicated a linear correlation between reaction rates and partial pressure of methanol. For this system, the value of activation energy ($E_a = \sim 36$ kJ mol^{-1}) obtained from the Arrhenius plot (Fig. 12) was found to be much lower than what is normally observed for various total and partial oxidation reactions.

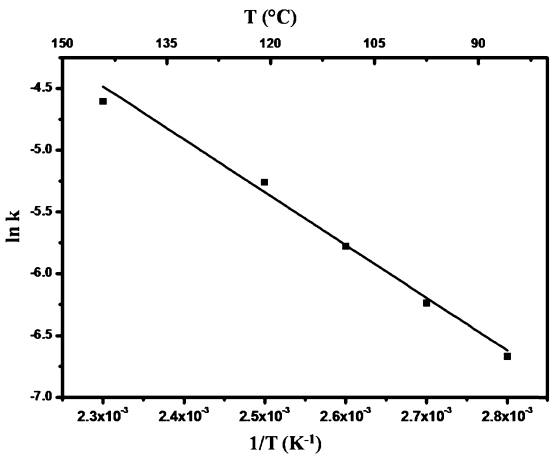

Fig. 12. Arrhenius plot of the rate constant k obtained for nanocast $LaMnO_3$ synthesized using KIT-6 aged at 100 °C as the hard template. Reprinted with permission from reference [37]. Copyright 2012 (Wiley).

In another study, a nanocast $LaMnO_3$ oxygen carrier demonstrated high reactivity under chemical looping combustion (CLC) conditions [39]. There, a series of perovskite-based oxygen carriers ($LaCoO_3$, $LaCeCoO_3$ and $LaMnO_3$) synthesized by reactive grinding and a nanocast $LaMnO_3$ synthesized from KIT-6 silica were compared. This nanocast material showed extremely high value of specific surface area (170 m^2 g^{-1}), retained even after subsequent calcination of the silica-free powder at 550 °C. TPD-O_2 and TPR-H_2 analysis confirmed the high amount of surface oxygen and high density of surface anion vacancies for the nanocast $LaMnO_3$ perovskite. The reactivity and stability of the perovskite-based oxygen carriers were tested in a *CREC Riser Simulator* equipment using methane as a reducing gas for combustion and air for regeneration of the reduced carriers. Combustion and regeneration were carried out at 650 °C under atmospheric pressure. The results of methane conversion versus the number of reduction–oxidation cycles on the Mn-based perovskite carrier synthesized by both methods showed small amount of CO, along with CO_2 and H_2O, and the average conversion of methane was found to be 77% over both carriers. The nanocast $LaMnO_3$ oxygen carrier demonstrated high reactivity during ten reduction–oxidation cycles under CLC conditions. However, the selectivity of methane combustion toward CO_2 was affected, as more CO was produced in this case. Indeed, the average selectivity toward CO was 22% for $LaMnO_3$ synthesized by nanocasting, while it was only 11% for the sample prepared by reactive grinding. In fact, a strong dependency of the catalytic efficiency on the CH_4 pressure was observed for these materials. Higher stability and no CO formation were observed during multiple redox cycles using low pressure of CH_4. On the other hand, while high reactivity was observed over some time at high CH_4 pressure, production of CO was detected. Also, coke formation is an obstacle which would limit the efficiency of the total CO_2 separation. Therefore, it is important to minimize its formation by selecting an appropriate oxygen carrier and adjusting the reaction conditions. In this study it was observed that the measured amount of carbon deposited on the oxygen carriers after the 10th reduction step remained negligibly small. The nanocast $LaMnO_3$ oxygen carrier demonstrated good stability under the repeated redox cycles although for the last cycles a small reduction in the methane conversion was observed. This decrease was attributed to the formation of a stable lanthanum silicate compound, which presence was confirmed by XRD. No coke formation was detected on these nanocast oxygen carriers, however, some agglomeration of the particles occurred.

4. Conclusions and perspectives

In this account, we have summarized some of the recent developments regarding the nanocasting synthesis

and catalytic applications of high surface area mixed metal oxides. The research conducted so far indicates that the nanocasting method is quite versatile for the synthesis of a variety of mesoporous mixed metallic compositions, especially on the basis of non-noble metals (Copper oxide, ceria, spinels, perovskites, etc.) using various templates (mesoporous silica and carbon). The thus-synthesized materials are highly efficient for low temperature gas-phase reactions ($< 150\,^{\circ}C$), such as the preferential oxidation of CO in excess H_2, or the total oxidation of methanol, as a model VOC. Furthermore, Cu/Ni-based nanocast materials showed excellent catalytic activity for hydrogen evolution from ammonia borane in aqueous phase under ambient conditions. Concerning high temperature efficiency, these materials are suitable catalysts for total oxidation of methane or chemical looping combustion in which simultaneous oxidation/reduction cycles are involved. Nevertheless, one of the main issues remaining to be solved in some cases (e.g., perovskites) is the presence of variable amounts of residual silicon, following the removal of the silica template. Yet, it remains difficult to precisely describe the role of these impurities on the efficiency or stability of the nanocast catalysts, and further studies are needed to clarify these aspects.

The recent advances in the area of nanocast materials illustrate very well how mixed metal compositions that are confined in high surface area nanostructures could indeed provide high catalytic efficiency and valuable synergetic effects, owing to the creation of favorable metal (oxide) interfaces in nano-domains. In turn, this should be of great significance for the design of cheaper new catalysts aiming at reactions which are crucial for energy and environmental purposes. Future research efforts regarding the utilization of nanocast mixed metal oxides for energy-specific applications are awaited. For instance, it will be highly interesting to study the catalytic properties of these compositions (perovskites especially) in reforming reactions, such as dry reforming or steam reforming, to produce syngas ($CO + H_2$) [109,110]. Alternatively, nanocast catalysts may also be tested in the conversion of syngas into value added chemicals, particularly oxygenated hydrocarbons such as alcohols. Another interesting area of perspectives for nanocast mesoporous mixed oxides is for electrocatalytic oxygen reduction/evolution reactions (ORR/OER) [111,112]. There, it is known that conventional (bulk) oxides with perovskite and spinel structures show promises for such applications [99,100]. Finally, these nanocast mixed oxides should also possess a vast potential for applications involving biomass conversion, especially with an emphasis on non-noble metal compositions whereby combination of properties (redox, acid–base, stabilization, etc.) may be achieved. Evidently, in spite of the multi-step templated nanocasting synthesis, there is a great potential for further development of nanostructured mixed metal oxide compositions, with prospects of applications in catalysis, as well as in other areas of materials science and nanotechnology [113].

Acknowledgements

This work was supported by NSERC (Canada) and FQRNT (Province of Québec). The authors thank Prof S. Kaliaguine (Department of Chemical Engineering, Université Laval, Québec, Canada) for helpful discussion and technical support.

References

[1] C.T. Kresge, M.E. Leonowicz, W.J. Roth, J.C. Vartuli, J.S. Beck, Nature 359 (1992) 710.
[2] P. Yang, D. Zhao, D.I. Margolese, B.F. Chmelka, G.D. Stucky, Nature 396 (1998) 152.
[3] Y. Meng, D. Gu, F. Zhang, Y. Shi, H. Yang, Z. Li, C. Yu, B. Tu, D. Zhao, Angew. Chem. Int. Ed. 44 (2005) 7053.
[4] F. Zhang, Y. Meng, D. Gu, Y. Yan, C. Yu, B. Tu, D. Zhao, J. Am. Chem. Soc. 127 (2005) 13508.
[5] A.H. Lu, B. Spliethoff, F. Schüth, Chem. Mater. 20 (2008) 5314.
[6] J.H. Knox, B. Kaur, G.R. Millward, J. Chromatogr. 352 (1986) 3.
[7] S. Jun, S.H. Joo, R. Ryoo, M. Kruk, M. Jaroniec, Z. Liu, T. Ohsuna, O. Terasaki, J. Am. Chem. Soc. 122 (2000) 10712.
[8] T.W. Kim, R. Ryoo, K.P. Gierszal, M. Jaroniec, L.A. Solovyov, Y. Sakamoto, O. Terasaki, J. Mater. Chem. 15 (2005) 1560.
[9] A. Rumplecker, F. Kleitz, E. Salabas, F. Schüth, Chem. Mater. 19 (2007) 485.
[10] F. Jiao, A.H. Hill, A. Harrison, A. Berko, A.V. Chadwick, P.G. Bruce, J. Am. Chem. Soc. 130 (2008) 5262.
[11] H. Tüysüz, M. Comotti, F. Schüth, Chem. Commun. 34 (2008) 4022.
[12] X. Liu, B. Tian, C. Yu, B. Tu, Z. Liu, O. Terasaki, D. Zhao, Chem. Lett. 32 (2003) 824.
[13] F. Gao, Q. Lu, D. Zhao, Adv. Mater. 15 (2003) 739.
[14] Y.F. Shi, Y. Meng, D.H. Chen, S.J. Cheng, P. Chen, T.F. Yang, Y. Wan, D. Zhao, Adv. Funct. Mater. 16 (2006) 561.
[15] Y.F. Shi, Y. Wan, R.Y. Zhang, D. Zhao, Adv. Funct. Mater. 18 (2008) 2436.
[16] A.H. Lu, F. Schüth, Adv. Mater. 18 (2006) 1793.
[17] H. Yang, D. Zhao, J. Mater. Chem. 15 (2005) 1217.
[18] F. Schüth, Chem. Mater. 13 (2001) 3184.
[19] M. Tiemann, Chem. Mater. 20 (2008) 961.
[20] T. Wagner, S. Haffer, C. Weinberger, D. Klaus, M. Tiemann, Chem. Soc. Rev. 42 (2013) 4036.
[21] Y. Ren, Z. Ma, P.G. Bruce, Chem. Soc. Rev. 41 (2012) 4909.
[22] D. Gu, F. Schüth, Chem. Soc. Rev. 43 (2014) 313.
[23] H. Yang, Q. Shi, B. Tian, Q. Lu, F. Gao, S. Xie, J. Fan, C. Yu, B. Tu, D.J. Zhao, Am. Chem. Soc. 125 (2003) 4724.
[24] B. Tian, X. Liu, L.A. Solovyov, Z. Liu, H. Yang, Z. Zhang, S. Xie, F. Zhang, B. Tu, C. Yu, O. Terasaki, D. Zhao, J. Am. Chem. Soc. 126 (2004) 865.
[25] K. Jiao, B. Zhang, B. Yue, Y. Ren, S. Liu, S. Yan, C. Dickinson, W. Zhou, H. He, Chem. Commun. 5618 (2005).
[26] C. Dickinson, W. Zhou, R.P. Hodgkins, Y. Shi, D. Zhao, H. He, Chem. Mater. 18 (2006) 3088.
[27] E.L. Salabas, A. Rumplecker, F. Kleitz, F. Radu, F. Schüth, Nano Lett. 6 (2006) 2977.
[28] F. Jiao, P.G. Bruce, Adv. Mater. 19 (2007) 657.
[29] F. Jiao, K.M. Shaju, P.G. Bruce, Angew. Chem. Int. Ed. 44 (2005) 6550.
[30] J. Shi, Chem. Rev. 113 (2013) 2139.
[31] M. Behrens, F. Studt, I. Kasatkin, S. Kühl, M. Hävecker, F. Abild-Pedersen, S. Zander, F. Girgdies, P. Kurr, B.-L. Kniep, M. Tovar, R.W. Fisher, J.K. Nørskov, R. Schlögl, Science 336 (2012) 893.
[32] D.A. Hansgen, D.G. Vlachos, J.G.G. Chen, Nat. Chem. 2 (2010) 484.
[33] F. Studt, F. Abild-Pedersen, T. Bligaard, R.Z. Sørensen, C.H. Christensen, J.K. Nørskov, Science 320 (2008) 1320.
[34] G.W. Huber, J.W. Shabaker, J.A. Dumesic, Science 300 (2003) 2075.
[35] H. Yen, Y. Seo, R. Guillet-Nicolas, S. Kaliaguine, F. Kleitz, Chem. Commun. 47 (2011) 10473.
[36] H. Yen, Y. Seo, S. Kaliaguine, F. Kleitz, Angew. Chem. Int. Ed. 51 (2012) 12032.
[37] M.M. Nair, F. Kleitz, S. Kaliaguine, ChemCatChem 4 (2012) 387.
[38] H. Yen, F. Kleitz, J. Mater. Chem. A 1 (2013) 14790.
[39] Z. Sarshar, F. Kleitz, S. Kaliaguine, Energy Environ. Sci. 4 (2011) 4258.
[40] J.H. Smatt, N. Schuwer, M. Jarn, W. Lindner, M. Linden, Micropor. Mesopor. Mater. 112 (2008) 308.
[41] S. Lepoutre, B. Julian-Lopez, C. Sanchez, H. Amenitsch, M. Linden, D. Grosso, J. Mater. Chem. 20 (2010) 537.

[42] J.H. Smatt, C. Weidenthaler, J.B. Rosenholm, M. Linden, Chem. Mater. 18 (2006) 1443.
[43] F.M. Sayler, A.J. Grano, J.H. Smatt, M. Linden, M.G. Bakker, Micropor. Mesopor. Mater. 184 (2014) 141.
[44] J.W. Geus, A.J. van Dillen, in: G. Ertl, H. Knözinger, F. Schüth, J. Weitkamp (Eds.), Handbook of Heterogeneous Catalysis, Wiley-VCH, 2008, p. 428.
[45] A.-H. Lu, D. Zhao, Y. Wan, Nanocasting: A Versatile Strategy for Creating Nanostructured Porous Materials, RSC Publishing, 2010.
[46] B.Z. Tian, X.Y. Liu, H.F. Yang, S.H. Xie, C.Z. Yu, B. Tu, D.Y. Zhao, Adv. Mater. 15 (2003) 1370.
[47] S.C. Laha, R. Ryoo, Chem. Commun. (2003) 2138.
[48] F. Jiao, A. Harrison, J.C. Jumas, A.V. Chadwick, W. Kockelmann, P.G. Bruce, J. Am. Chem. Soc. 128 (2006) 5468.
[49] Y. Wan, D. Zhao, Chem. Rev. 107 (2007) 2811.
[50] X. Gu, W. Zhu, C. Jia, R. Zhao, W. Schmidt, Y. Wang, Chem. Commun. 47 (2011) 5337.
[51] J. Roggenbuck, T. Waitz, M. Tiemann, Micropor. Mesopor. Mater. 113 (2008) 575.
[52] Y.M. Wang, Z.Y. Wu, H.J. Wang, J.H. Zhu, Adv. Funct. Mater. 16 (2006) 2374.
[53] W.B. Yue, W.Z. Zhou, J. Mater. Chem. 17 (2007) 4947.
[54] K. Zhu, B. Yue, W. Zhou, H. He, Chem. Commun. (2003) 98.
[55] Y. Wang, C.-M. Yang, W. Schmidt, B. Spliethoff, E. Bill, F. Schüth, Adv. Mater. 17 (2005) 53.
[56] D. Myers, Surfaces, Interfaces, and Colloids, Wiley-VCH, 1999.
[57] M. Imperor-Clerc, D. Bazin, M.-D. Appay, P. Beaunier, A. Davidson, Chem. Mater. 16 (2004) 1813.
[58] X. Sun, Y. Shi, P. Zhang, C. Zheng, X. Zheng, F. Zhang, Y. Zhang, N. Guan, D. Zhao, G.D. Stucky, J. Am. Chem. Soc. 133 (2011) 14542.
[59] S.-Y. Lee, R. Aris, Catal. Rev. 27 (1985) 207.
[60] J.R.A. Sietsma, J.D. Meeldijk, J.P. den Breejen, M. Versluijs-Helder, A.J. van Dillen, P.E. de Jong, K.P. de Jong, Angew. Chem. Int. Ed. 46 (2007) 4547.
[61] J.R.A. Sietsma, J.D. Meeldijk, M. Versluijs-Hleder, A. broersma, A. Jos van Dillen, P.E. de Jong, K.P. de Jong, Chem. Mater. 20 (2008) 2921.
[62] M. Schwickardi, T. Johann, W. Schmidt, F. Schuth, Chem. Mater. 14 (2002) 3913.
[63] T. Valdes-Solis, G. Marben, A.B. Fuertes, Chem. Mater. 17 (2005) 1919.
[64] Y. Sun, G. Ji, M. Zheng, X. Chang, S. Li, Y. Zhang, J. Mater. Chem. 20 (2010) 945.
[65] H. Tüysüz, C.W. Lehmann, H. Bongarg, B. Tesche, R. Schmidt, F. Schüth, J. Am. Chem. Soc. 130 (2008) 11510.
[66] H. Tüysüz, E.L. Salabas, E. Bill, H. Bongard, B. Spliethoff, C.W. Lehmann, F. Schüth, Chem. Mater. 24 (2012) 2493.
[67] H. Tüysüz, C. Weidenthaler, F. Schüth, Chem. Eur. J. 18 (2012) 5080.
[68] Y. Ren, Z. Ma, L. Qian, S. Dai, H. He, P.G. Bruce, Catal. Lett. 131 (2009) 146.
[69] M. Jin, J.-N. Park, J.K. Shon, J.H. Kim, Z. Li, Y.-K. Park, J.M. Kim, Catal. Today 185 (2012) 183.
[70] D. Gu, C.-J. Jia, H. Bongard, B. Spliethoff, C. Weidenthaler, W. Schmidt, F. Schüth, Appl. Catal. B: Environ. 152–153 (2014) 11.
[71] S. Alayoglu, A.U. Nilekar, M. Mavrikakis, B. Eichhorn, Nat. Mater. 7 (2008) 333.
[72] A.U. Nilekar, S. Alayoglu, B. Eichhorn, M. Mavrikakis, J. Am. Chem. Soc. 132 (2010) 7418.
[73] Q. Fu, W.X. Li, Y. Yao, H. Liu, H.Y. Su, D. Ma, X.K. Gu, L. Chen, Z. Wang, H. Zhang, B. Wang, X. Bao, Science 328 (2010) 1141.
[74] A. Stephen, K. Hashmi, G.J. Hutchings, Angew. Chem. Int. Ed. 45 (2006) 7896.
[75] M. Comotti, W. Li, B. Spliethoff, F. Schuth, J. Am. Chem. Soc. 128 (2006) 917.
[76] P. Broqvist, I. Panas, H. Persson, J. Catal. 210 (2002) 198.
[77] J. Jansson, A.E.C. Palmqvist, E. Fridell, M. Skoglundh, L. Osterlund, P. Thormahlen, V. Langer, J. Catal. 211 (2002) 387.
[78] Y.Z. Wang, Y.X. Zhao, C.G. Ga, D.S. Liu, Catal. Lett. 116 (2007) 136.
[79] W. Shen, X. Dong, Y. Zhu, H. Chen, J. Shi, Micropor. Mesopor. Mater. 85 (2005) 157.
[80] J.K. Zhu, Q.M. Gao, Micropor. Mesopor. Mater. 124 (2009) 144.
[81] G. Avgouropoulos, T. Ioannides, Appl. Catal., B 67 (2006) 1.
[82] C.S. Polster, H. Nair, C.D. Baertsch, J. Catal. 266 (2009) 308.
[83] Y. Zhang, H. Liang, X.Y. Gao, Y. Liu, Catal. Commun. 10 (2009) 1432.
[84] E.D. Park, D. Lee, H.C. Lee, Catal. Today 139 (2009) 280.
[85] J.L. Cao, Y. Wang, X.L. Yu, S.R. Wang, S.H. Wu, Z.Y. Yuan, Appl. Catal., B 79 (2008) 26.
[86] L. Schlapbach, A. Züttel, Nature 414 (2001) 353.
[87] J. Yang, A. Sudik, C. Wolverton, D.J. Siegelw, Chem. Soc. Rev. 39 (2010) 656.
[88] A. Staubitz, A.P.M. Robertson, I. Manners, Chem. Rev. 110 (2010) 4079.
[89] C.W. Hamilton, R.T. Baker, A. Staubitz, I. Manners, Chem. Soc. Rev. 38 (2009) 279.
[90] M. Yadav, Q. Xu, Energy Environ. Sci. 5 (2012) 9698.
[91] P.Z. Li, A. Aijaz, Q. Xu, Angew. Chem. Int. Ed. 51 (2012) 6753.
[92] O. Metin, V. Mazumder, S. Özkar, S. Sun, J. Am. Chem. Soc. 132 (2010) 1468.
[93] S.B. Kalidindi, M. Indirani, B.R. Jagirdar, Inorg. Chem. 47 (2008) 7424.
[94] Y. Yamada, K. Yano, Q. Xu, S. Fukuzumi, J. Phys. Chem. C 114 (2010) 16456.
[95] Y. Yamada, K. Yano, S. Fukuzumi, Energy Environ. Sci. 5 (2012) 5356.
[96] Q. Xu, M. Chandra, J. Power Sources 163 (2006) 364.
[97] X. Yang, F. Cheng, J. Liang, Z. Tao, J. Chen, J. Power Sources 34 (2009) 8785.
[98] R. Yi, R. Shi, G. Gao, N. Zhang, X. Cui, Y. He, X. Liu, J. Phys. Chem. C 113 (2009) 1222.
[99] J. Suntivich, K.J. May, H.A. Gasteiger, J.B. Goodenough, Y. Shao-Horn, Science 334 (2011) 1383.
[100] J. Suntivich, H.A. Gasteiger, N. Yabuuchi, H. Nakanishi, J.B. Goodenough, Y. Shao-Horn, Nat. Chem. 3 (2011) 546.
[101] Y. Wakabayashi, M.H. Upton, S. Grenier, J.P. Hill, C.S. Nelson, J.W. Kim, P.J. Ryan, A.I. Goldman, H. Zheng, J.F. Mitchell, Nat. Chem. 6 (2007) 972.
[102] D.B. Meadowcroft, Nature 226 (1970) 847.
[103] L.A. Pedersen, W.F. Libby, Science 176 (1972) 1355.
[104] M.A. Pena, J.L.G. Fierro, Chem. Rev. 101 (2001) 1981.
[105] H. Arai, T. Yamada, K. Eguchi, T. Seiyama, Appl. Catal. 26 (1986) 265.
[106] C.H. Kim, G. Qi, K. Dahlberg, W. Li, Science 327 (2010) 1624.
[107] Y. Wang, J. Ren, Y. Wang, F. Zhang, X. Liu, Y. Guo, G. Lu, J. Phys. Chem. C 112 (2008) 15293.
[108] R.K.C. de Lima, M.S. Batista, M. Wallau, E.A. Sanches, Y.P. Mascarenhas, E.A. Urquita-Gonzalez, Appl. Catal., B 90 (2009) 441.
[109] N. Wang, X. Yu, Y. Wang, W. Chu, M. Liu, Catal. Today 212 (2013) 98.
[110] M.M. Nair, S. Kaliaguine, F. Kleitz, submitted.
[111] H. Tüysüz, Y.J. Hwang, S.B. Khan, A.M. Asiri, P. Yang, Nano Res. 6 (2013) 47.
[112] Y.J. Sa, K. Kwon, J.Y. Cheon, F. Kleitz, S.H. Joo, J. Mater. Chem. A 1 (2013) 9992.
[113] F. Jiao, H. Yen, G.S. Hutchings, B. Yonemoto, Q. Lua, F. Kleitz, J. Mater. Chem. A 2 (2014) 3065.